Nuclear Instruments and Methods in Physics Research B 331 (2014) 140–143

Contents lists available at ScienceDirect

Nuclear Instruments and Methods in Physics Research B

journal homepage: www.elsevier.com/locate/nimb

Ion beam modification of the structure and properties of hexagonal boron nitride: An infrared and X-ray diffraction study

E. Aradi *, S.R. Naidoo, D.G. Billing, D. Wamwangi, I. Motochi, T.E. Derry

DST/NRF Centre of Excellence in Strong Materials, the School of Physics and the School of Chemistry, University of the Witwatersrand, Private Bag 3 Wits 2050, Johannesburg, South Africa

ARTICLE INFO

Article history:
Received 30 September 2013
Received in revised form 21 January 2014
Accepted 22 January 2014
Available online 11 March 2014

Keywords:
Ion implantation
Boron nitride
Glancing incidence XRD
Fourier Transform Infrared Spectroscopy

ABSTRACT

The vibrational mode for the cubic symmetry of boron nitride (BN) has been produced by boron ion implantation of hexagonal boron nitride (*h*-BN). The optimum fluence at 150 keV was found to be 5×10^{14} ions/cm^2. The presence of the *c*-BN phase was inferred using glancing incidence XRD (GIXRD) and Fourier Transform Infrared Spectroscopy (FTIR). After implantation, Fourier Transform Infrared Spectroscopy indicated a peak at 1092 cm^{-1} which corresponds to the vibrational mode for nanocrystalline BN (nc-BN). The glancing angle XRD pattern after implantation exhibited *c*-BN diffraction peaks relative to the implantation depth of 0.4 μm.

1. Introduction

The unique characteristics exhibited by cubic boron nitride [1–5] have led to a great deal of research with an aim of synthesizing it under less extreme conditions of pressure and temperature. Previous work has shown evidence that the cubic phase could be induced from the hexagonal BN (*h*-BN) phase by the ion implantation process and was identified primarily by Raman Spectroscopy [6,7]. The Raman spectroscopy after implantation showed additional phonon peaks at wavenumbers between 1295 cm^{-1} and 1303 cm^{-1} which were assigned to the sp^3 phonon mode for *c*-BN phase together with the *h*-BN principal peaks at 1366 cm^{-1}. The ion implantation process also offers the advantage of creating thin hardened layers under the surface of a previously shaped component. In this additional techniques were used to analyze the implanted *h*-BN to further corroborate the results from [7,8].

Fourier Transform Infrared Spectroscopy and Glancing incidence X-ray diffraction were used here to analyze the *h*-BN samples before and after implantation to establish the presence of nc-BN. FTIR was applied in order to identify the local structural order, functional groups and composition of the sample before and after implantation as it is sensitive to the local hybridization of the sp^2 and sp^3 phases of BN [9]. GIXRD is used to understand the morphology of the crystal structure. We use glancing angle in contrast to the conventional XRD because of its depth profiling capabilities since the implanted layer extends from the surface to a few hundred nanometres below the sample surface [10].

2. Experimental

2.1. Sample and sample preparations

The *h*-BN samples which were used throughout this experiment were hot pressed polycrystalline sheets supplied by the Goodfellow Cambridge Company, England, with dimensions of $5 \times 5 \times 0.2$ mm^3 and 99.9% purity. The samples were prepared by reaction of boric acid with urea followed by sintering using boron oxide and subsequent machining. The samples were cut using our Model 3032 Diamond Saw to a thickness of 0.1 mm and mechanically polished down to 0.05 mm on the side that was cut by the diamond wire saw. The implantation was performed on the originally hot pressed surface of the sample.

2.2. Ion implantation

A Varian 200-20A2F ion implanter located at iThemba LABS (Gauteng), in Johannesburg, was used for the implantation experiments. All implants were done at room temperature using B^+ at energy of 150 keV at a dose rate of $\approx 10^{13}$ ions/s. The B^+ ions were obtained from boron trifluoride gas ionized in the ion source chamber of the ion implanter and selected by the implanter's mass analyzer magnet. Analyses of the samples were carried out before and after implantation using the Bruker TENSOR 27 Fourier Transform

* Corresponding author. Tel.: +27 794020582.
E-mail address: aradi.emily@gmail.com (E. Aradi).

http://dx.doi.org/10.1016/j.nimb.2014.01.031
0168-583X/

Infra-red spectrometer and the D8 ADVANCED Bruker X-ray Diffractometer at the University of the Witwatersrand. The X-ray diffractometer was set to operate at a voltage of 40 kV and 40 mA current. Measurements were carried out in the 2θ mode at glancing incident angles ranging from 0.01° to 0.5° from $2\theta = 20°$ to 90° in steps of at 0.05° per second. The CuKα anticathode with wavelength of 1.5406 Å was used to perform all the XRD measurements.

3. Results and discussions

3.1. Fourier Transform Infrared Spectroscopy (FTIR)

Fig. 1(a) represents the FTIR transmission spectrum for the sample before implantation. The spectrum shows two distinct modes at 778 cm^{-1} and 1374 cm^{-1}. These vibrational modes have been attributed to the sp^2 bonded *h*-BN. The mode at 778 cm^{-1} represents the A_{lu} out-of-plane bending vibration while the mode at 1374 cm^{-1} is the E_{lu} in-plane stretching vibration for *h*-BN also observed by [11]. There were no other modes visible in the unimplanted spectra.

After implantation, the A_{lu} and E_{lu} mode were still visible but they show a frequency shift to higher wavenumber of 784 cm^{-1} and 1382 cm^{-1}, respectively after implantation. The peak shift to higher wavenumbers implies that there is compresive stress accumulation in the material as a result of radiation damage caused by the implantation [12].

Together with the *h*-BN vibrational modes, another phonon peak is observed at 1092 cm^{-1} (arrowed) in Fig. 1(b) after implantation. This peak has been observed to represent the TO mode for sp^3 nc-BN [13]. The frequency mode of the *c*-BN is dependent on the particle size, impurity level and the stress level in the material [14]. For *c*-BN with no internal stress, the peak is centred at 1000 cm^{-1} [15]. For bulk samples with residual compressive stress, the peak occurs at 1050 cm^{-1} and as the crystal size decreases to a nanoscale, the peak shifts to higher wavenumbers of between 1090 cm^{-1} and 1120 cm^{-1} [16]. From this information, it is suggested that nc-BN particles or regions are formed in the implanted layer complementing the Raman results reported in [8].

Also observed is a slight split of the *h*-BN E_{lu} mode after implantation forming another peak centred at 1388 cm^{-1}. We tentatively attribute this mode to the rhombohedral/*r*-BN vibrational mode which may have been induced due to the distortion of the *h*-BN lattice as a result of the radiation damage created during the implantation [17]. An additional feature is also observed at 938 cm^{-1} whose origin is unknown.

A fluence dependent analysis at 150 keV was carried out on the samples by implanting them with boron at various fluences to investigate the effect of varying the defect density in the implanted layer. We assume that little or no self annealing takes place during the implantation process and hence increasing the dose increases the damage density in the implanted region.

The fluence dependence of the TO mode for the nc-BN production is shown in Fig. 2. In the spectra the *h*-BN modes have been cut off so as to bring the peak associated with nc-BN to a clear view. The peaks are centred at 1098 cm^{-1}, 1092 cm^{-1} and 1105 cm^{-1} for the respective fluences. The integrated peak intensity shows the highest intensity of the TO mode at 5×10^{14} ions/cm^2 and decreased when the dose was increased to 1×10^{15} ions/cm^2.

Fourier Transform IR transmission intensities have been used to obtain the estimated amount of *c*-BN in a hexagonal-cubic mixed phase sample. This has been achieved using intensities of the peaks as indicated in the equation below [18]:

$$\%(c\text{-BN}) = \frac{I_{c\text{-BN}}}{(I_{c\text{-BN}} + I_{h\text{-BN}})} \times 100 \quad (1)$$

where $I_{c\text{-BN}}$ is the integrated transmission intensity for *c*-BN for the respective wavenumbers in the mixed phase and $I_{h\text{-BN}}$ is the integrated intensity for the *h*-BN principal peak before implantation at 1374 cm^{-1}.

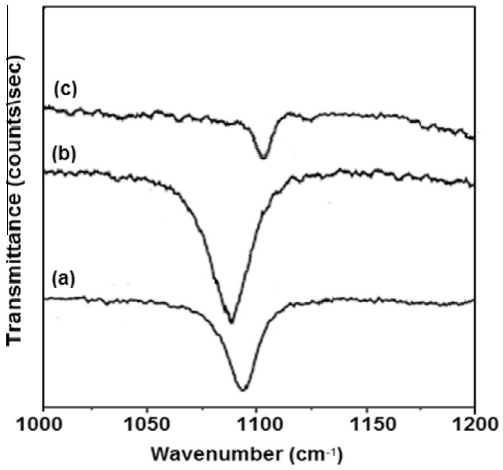

Fig. 2. FTIR spectrum for samples implanted at (a) 1×10^{14} ions/cm^2 (b) 5×10^{14} ions/cm^2 and (c) 1×10^{15} ions/cm^2.

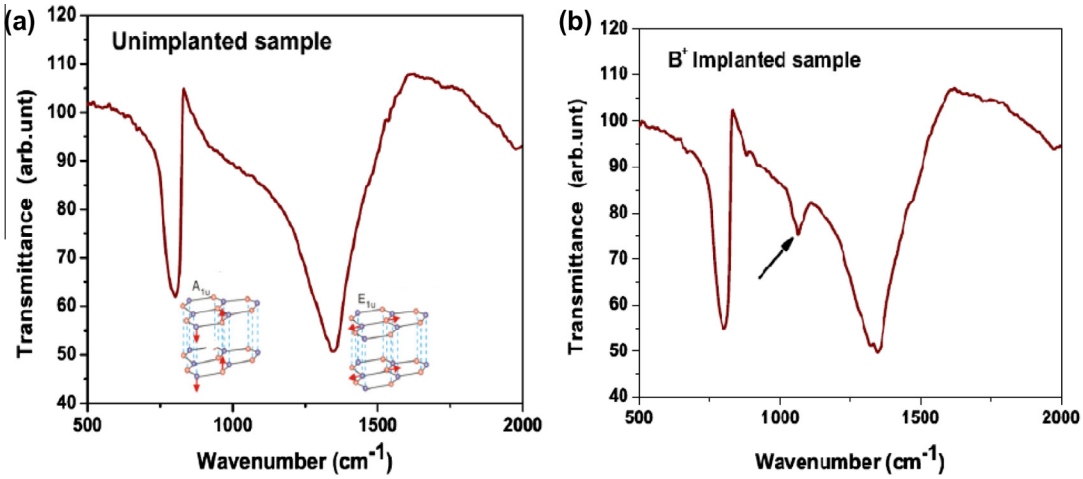

Fig. 1. Fourier Transform Infrared spectrum for (a) unimplanted *h*-BN and (b) *h*-BN implanted with boron ions at 5×10^{14} ions/cm^2 at 150 keV.

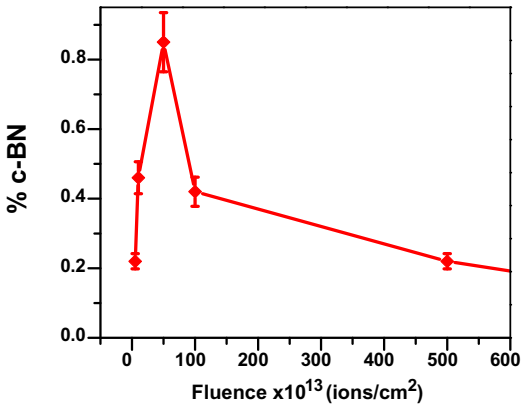

Fig. 3. Estimated amount of *c*-BN produced as a function of the fluence for samples implanted with boron at 150 keV. (Additional fluences are included).

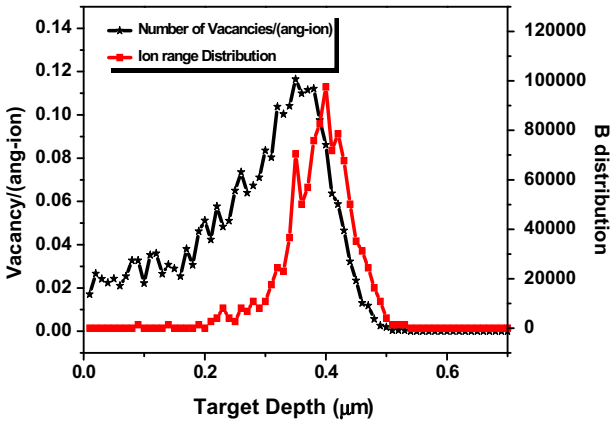

Fig. 4. SRIM simulation results for the number of vacancies and the ion distribution as a function of target depth the for *h*-BN implanted with B^+ ions at 150 keV.

From these observations, an implanted dose of 5×10^{14} ions/cm^{-1} gave the highest estimated percentage of nc-BN of all the fluences. The amount decreases substantially for the high fluences and also noted (not shown in figure) is that at even higher fluence of 5×10^{16} ions/cm^2, no *c*-BN mode is detected. This observation suggests that there is threshold fluence below and above which no nc-BN could be detected. A similar trend has been observed and recorded using Raman spectroscopy analysis [6]. After reaching the optimum value, any more ions introduced into the material leads to more stress as a result of the increase in radiation damage. This increased stress and radiation damage results in a decrease in both the vibrational modes of both the sp^2 and sp^3 BN bonds and in our case the total extinction of the sp^3 vibrational modes. Based on these observations, it is suggested that the sp^3 phase is probably stress induced in the implanted layer and this induced phase has a threshold related to the defect density in the implanted layer (see Fig. 3).

3.2. Glancing Incidence X-ray Diffraction

Glancing incidence XRD was also used to identify the structure and lattice parameter of the material before and after implantation. All the GIXRD measurements presented here are for the glancing incident angle of 0.3° which is above the total external reflection edge of BN [19]. This angle also corresponds to a penetration depth where the X-rays diffract from the implanted layer of *h*-BN.

The normal penetration depth of the X-rays in *h*-BN at the incident angle of 0.3° is calculated to be 0.38 μm [20]. Simulations using the Stopping and Range of Ions in Matter programme (SRIM) 2008 [21] for the ion distribution and number of vacancies created in *h*-BN implanted with B^+, at 150 keV is shown in Fig. 4. It gives a projected range for the ions to be ≈0.4 μm and the damage extends to a depth of ≈0.5 μm.

Fig. 5 shows the diffraction pattern for *h*-BN samples before and after implantation, with the first figure showing diffraction angles from 40° to 55° and the second figure from 55° to 90° for the same sample. This was done to show clearly the features with low intensities relative to the principal *h*-BN peak. Fig. 5(a) shows the different diffraction peaks at $2\theta = 41.8°$, 43.9°, 50.2°, 55.2, 78° and 82° corresponding to planes (100), (101), (102) (004), (110) and (112) of an essentially homogeneous and randomly oriented *h*-BN with lattice parameters $a = 2.504$ Å and $c = 6.662$ Å [22].

After implantation, the *h*-BN diffraction peaks observed are still prevalent in the GIXRD pattern. Together with these, new peaks at 43.3°, 63.3°, 74.37° and 89.3° are observed. The peak at 63.3° has been associated with the (015) plane of rhombohedral BN phase. Rhombohedral BN has initially been produced transitionally during the *h*-BN to *c*-BN phase transformation [23]. These phase has also been observed with FTIR analyses presented in the previous section. It is a challenge to observe the *r*-BN mode with Raman spectroscopy for a mixed BN phase since the phonon mode is very close to and often overlaps with the *h*-BN mode at 1367 cm^{-1} [17].

The other three peaks, located at 43.3°, 74.37° and 89.3° have been calculated and found to represent the (111), (220) and the (311) planes for *c*-BN, with lattice parameter $a = 3.615$ Å, and

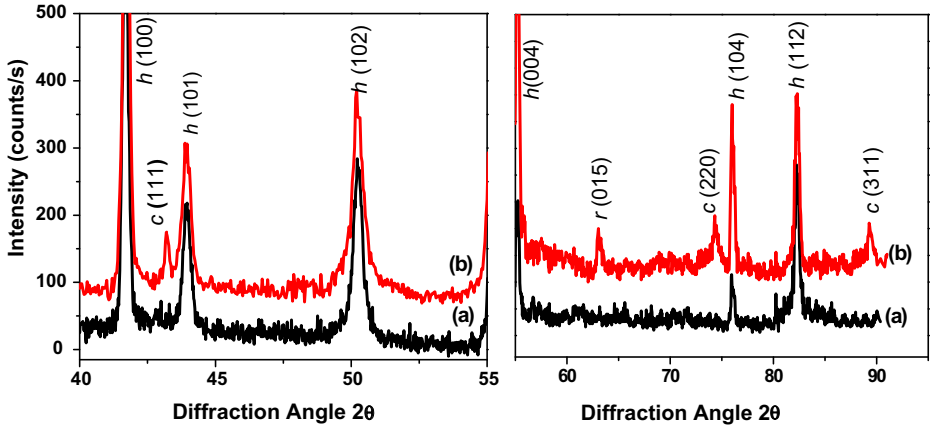

Fig. 5. GIXRD pattern for *h*-BN (a) before implantation and (b) after implantation with boron ions at 5×10^{14} ions/cm^2 and energy of 150 keV.

a = 3.616 Å and a = 3.614 Å respectively, with similar values compared to JCPDS database (no. 35-1365) and also reported by [24,25]. The wurtzite BN, with lattice parameters $a = b = 2.55$ Å and $c = 4.2154$ Å, normally exhibits diffraction at 74° and in analysis it can be easily confused with the c-BN peak. We do not attribute this to the wurtzite phase since no evidence has been seen in any of the optical spectroscopy used in this study and previous work.

The peaks are of low intensity with a broad linewidth with respect to the h-BN peaks indicating that the c-BN could be of nanosized particles or regions, agreeing well with results from FTIR. Assuming that they are spherical, it is possible to estimate the particle size of the material with XRD by assuming that the line broadening will be due to the reduced particle size. Using the Scherrer equation [26]:

$$D_{\text{crystal}} = \frac{k\lambda}{\beta_{1/2}\cos\theta} \tag{2}$$

where k is the shape constant factor $k \sim 0.94$, $\lambda = 1.5406$ nm is the wavelength of radiation (in our case for CuKα), and $\beta_{1/2}$ the line width at half maximum for the c-BN peak; the particle size for c-BN was estimated to be ~9 nm for the sample that was implanted with boron at 5×10^{14} ions/cm^2. A dose dependent analysis (not shown in this work) will be used to determine whether the observed line broadening is stress related.

Analyses using HRTEM have been a challenge and initial results shown in [7] are part of an ongoing study. Focused Ion beam Milling sample preparation for HRTEM has been difficult due to the porosity of the hot pressed samples used thus far.

4. Conclusion

Further evidence from FTIR and GIXRD strongly suggest that sp^3 bonded BN can be induced in h-BN after implantation with boron ions. The best results were obtained at a fluence of 5×10^{14} ions/cm^2 for the energy of 150 keV. Rhombohedral BN vibrational mode of BN have also been observed after implantation.

Acknowledgement

The authors are grateful to DST/NRF Centre of Excellence in Strong Materials for financial support and iThemba LABS (Gauteng) for the use of the Ion Implanter.

References

[1] S.N. Monteiro, A.L.D. Skury, M.G. de Azevedo, G.S. Bobrovnitchi, J. Mater. Res. Technol. 2 (2013) 68.
[2] Q. Li, S.F. Wong, W.M. Lau, C.W. Ong, Diamond Relat. Mater. 16 (2007) 421.
[3] P. Huang, M. Wong, Vacuum 100 (2014) 66.
[4] O. Lehtinen, T. Nikitin, A.V. Krasheninnikov, Phys. Status Solidi C 7 (2010) 1256.
[5] W.J. Zhang, Y.M. Chong, I. Bello, S.T. Lee, J. Phys. D: Appl. Phys. 40 (2007) 6159.
[6] R. Machaka, R.M. Erasmus, T.E. Derry, Diamond Relat. Mater. 19 (2010) 11331.
[7] E. Aradi, S.R. Naidoo, R.M. Erasmus, B. Julies, T.E. Derry, Nucl. Instr. Meth. Phys. Res. B 307 (2013) 214.
[8] E. Aradi, R.M. Erasmus, T.E. Derry, Nucl. Instr. Meth. Phys. Res. B 272 (2012) 57.
[9] O. Kutsay, C. Yana, Y.M. Chong, Q. Ye, I. Bello, W.J. Zhang, J.A. Zapiena, Z.F. Zhoub, Y.K. Li, V. Garashchenko, A.G. Gontar, N.V. Novikov, S.T. Lee, Diamond Relat. Mater. 19 (2010) 968.
[10] W.C. Marra, P. Eisenberger, A.Y. Cho, J. Appl. Phys. 50 (1979) 6927.
[11] B. Fakrach, A. Rahmani, H. Chadli, K. Sbai, M. Bentaleb, Phys. Rev. 85 (2012) 115437.
[12] Y. Liu, P. Jin, A. Chen, H. Yang, Y. Xu, J. Appl. Phys. 112 (2012) 053501–053502.
[13] M.G. Beghi, C.E. Bottani, A. Miotello, P.M. Ossi, Thin Solid Films 308–309 (1997) 107.
[14] X.P. Hao, D.L. Cui, G.X. Shi, Y.Q. Yin, X.G. Xu, J.Y. Wand, M.H. Jiang, X.W. Xu, Y.P. Li, B.Q. Sun, Chem. Mater. 13 (2001) 2457.
[15] P.M. Ossi, A. Miotello, Appl. Organomet. Chem. 15 (2001) 430.
[16] P.W. Zhu, Y.N. Zhao, B. Wang, Z. He, D.M. Li, G.T. Zou, J. Solid State Chem. 167 (2002) 420.
[17] P.B. Mirkarimi, K.F. McCathy, D.L. Medlin, Mater. Sci. Eng. R 21 (1997) 47.
[18] C.B. Samantaray, R.N. Singh, Int. Mater. Rev. 50 (2005) 313.
[19] B. Abendroth, R. Gago, F. Eichhorn, W. Möller, Appl. Phys. Lett. 85 (24) (2004) 5905.
[20] T. Mshino, T. Matsumoto, K. Nakamae', Polym. Eng. Sci. 40 (2000) 336.
[21] J.F. Ziegler, http://www.srim.org, (26.10.2013).
[22] M.-S. Jin, N.-O. Kim, J. Elec, Eng. Technol. 5 (4) (2010) 637.
[23] H. Saitoh, W.A. Yarbrough, Appl. Phys. Lett. 15 (1991) 2228.
[24] W.J. Zhang, S. Matsumoto, Phys. Rev. B 63 (2001) 073201.
[25] S. Ulrch, E. Nold, K. Sell, M. Stüber, J. Ye, C. Ziebert, Surf. Coat. Technol. 200 (2006) 6465.
[26] W. Gissler, J. Haupt, A. Hoffmann, P.N. Gibson, D.G. Rickerby, Thin Solid Films 199 (1991) 113.